Composite Structures 100 (2013) 280–289

Contents lists available at SciVerse ScienceDirect

Composite Structures

journal homepage: www.elsevier.com/locate/compstruct

Buckling behavior of curved composite beams with different elastic response in tension and compression

Fernando Fraternali *, Saverio Spadea, Luigi Ascione

Department of Civil Engineering, University of Salerno, Via Ponte Don Melillo, 84084 Fisciano, SA, Italy

ARTICLE INFO

Article history:
Available online 8 January 2013

Keywords:
Curved beams
Fiber-reinforced composites
Buckling
Bimodular behavior

ABSTRACT

A geometrically nonlinear finite element model of a composite curved beam is presented, accounting for moderately large rotations of the cross-sections, moderately large shear strains, small axial strains, and different elastic response of the material in tension and compression (bimodular behavior). A path following procedure in displacement control is employed to compute the stability points and the post-buckling response of the given model. Several comparisons are established with different numerical approaches available in the literature, showing the accuracy of the proposed finite element scheme in the unimodular case. Some original results on the in-plane and out-of-plane buckling of bimodular arches highlight that the post-buckling response of such structures is strongly influenced by the ratios between tensile and compressive moduli.

1. Introduction

Over the last two decades, fiber reinforced composites have received considerable attention in the field of civil engineering. Due to their light weight, high tensile strength and corrosion resistance, fiber reinforced polymers (FRPs) have been extensively employed in combination with other traditional construction materials, mostly for structural retrofitting and concrete reinforcement [1–3]. Full FRP profiles have been employed as nonstructural elements (pipes, waterspouts, gutters, etc.), and for the construction of bridge structures [4–6]. Other composite materials that are receiving increasing attention in the area of civil engineering are fiber-reinforced concretes and mortars. In this case, the addition of reinforcing fibers to the mix design may lead to significant increases of basic properties of the final composite material, such as, e.g., thermal resistance, tensile strength and material toughness (refer to [7–9] and therein references). Regarding the shape of composite profiles, it is worth noting that curved beams bear a special relevance in the construction industry [10–16], since such elements can be used to form special light-weight roof structures and arch bridges [17,18].

Due to their characteristic slenderness, composite beams usually need to be designed to prevent buckling more than material failure. The available literature on the elastic stability of such elements is mainly focused on thin-walled members, and the combined effects of local and global buckling phenomena [19–22]. Their mechanical behavior has been modeled through different approaches over the last years, both in statics and dynamics, with special focus on stress analysis, shear and warping deformation, and geometrical nonlinearities [23–27]. The buckling behavior of composite elements with different elastic response in tension and compression (hereafter referred to as "bimodular" behavior [28,29]) has instead received limited attention in the literature to-date. Nevertheless, depending on the relative stiffness and strength of matrix and fibers, the moisture content, and other factors, the elastic moduli of several real (artificial or natural) composites may be either greater in tension than in compression, or vice versa (refer to [28–31] and therein references). The study of such a phenomenon in fiber-reinforced concretes and mortars awaits special attention, in combination with the analysis of different material strengths in tension and compression, to be carried out via crack-bridging methods and variational fracture models [32–34].

The present work investigates on the stability of laminated curved beams made up of composite materials showing different elastic moduli in tension and compression. Use is made of a single-layer version of the geometrically nonlinear theory presented in [35], which accounts for moderately large rotations of the cross-sections, moderately large shear strains, and small axial strains along the beam axis (cf. Section 2). The finite element approximation of such a theory (provided in Section 3) is based on Lagrangian isoparametric elements, a path-following procedure inspired by Batoz and Dhatt [35,36] and a bordering algorithm for the computation of stability points [37,38]. The fiber-governed constitutive model by Bert [29] is employed to capture the bimodular response of the material. The numerical results presented in Section 4 show the accuracy of the proposed finite element scheme, by establishing comparisons with available theoretical and numerical

* Corresponding author. Tel.: +39 089 964083; fax: +39 089 964045.
E-mail address: f.fraternali@unisa.it (F. Fraternali).

0263-8223/$ - see front matter © 2013 Elsevier Ltd. All rights reserved.
http://dx.doi.org/10.1016/j.compstruct.2012.12.021

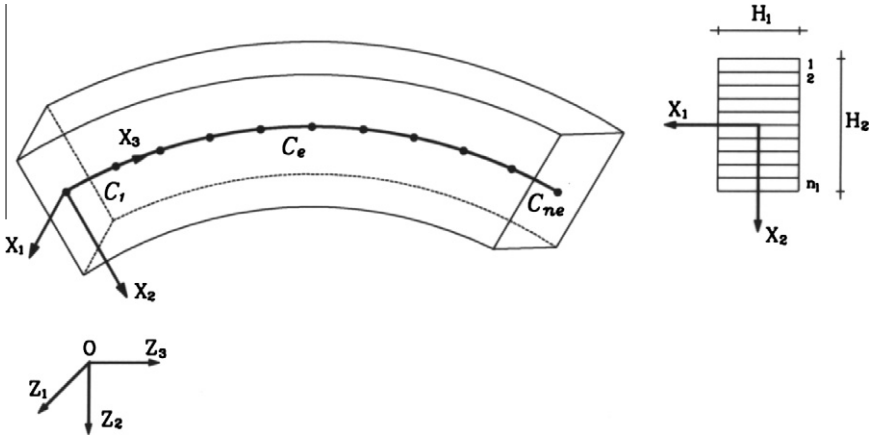

Fig. 1. Finite element approximation of the beam axis.

results for both unimodular [39,40] and bimodular case [41]. Some original results on the buckling behavior of bimodular composite arches are also given, highlighting some of the main features of the bimodular response of such structures in the post-buckling range. The conclusions of the present study are drawn in Section 5.

2. Kinematical model

Let us examine the deformation of a laminated beam from a stress-free reference configuration B_0 (Fig. 1). Throughout the paper, we let C denote the plane curve corresponding to the axis of B_0 and $S \in [0,L]$ the associated curvilinear abscissa. In addition, we let $\mathbf{A}_1$ denote the unit binormal vector; $\mathbf{A}_2$ the unit normal vector; and $\mathbf{A}_3$ and the unit tangent vector to C (Frenet frame).

The kinematic model adopted in the present work corresponds to a single-layer version of that presented in [35], which is based on the following basic assumptions:

- the beam axis is a plane curve;
- the beam is loaded by forces acting either in the axis-plane or out of the axis-plane;
- the beam axis may have arbitrarily large curvature;
- the generic cross-section remains unstrained in its own plane, but can feature out-of-plane warping.

Accordingly, we describe a generic deformation of the beam through the following displacement field [35]

$$\mathbf{u}(X_1,X_2,S) = \mathbf{v}(S) + [\mathbf{R}(S) - \mathbf{I}][X_1\mathbf{A}_1(S) + X_2\mathbf{A}_2(S)] + w_{r_1r_2}(S)X_1^{r1}X_2^{r2}\mathbf{A}_3(S) \quad (1)$$

where

- $\mathbf{v}(S)$ is the displacement field of the beam axis C;
- $\mathbf{R}(S)$ is the field of the rotation tensors of the cross-sections;
- $\mathbf{I}$ is the identity tensor;
- X_1 and X_2 are the coordinates of an arbitrary point of the current cross-section $\Sigma(S)$ with respect to $\mathbf{A}_1$ and $\mathbf{A}_2$, respectively;
- $w_{r_1r_2}(S)$ is the warping coefficient defined as the partial derivative of order $|r| = r_1 + r_2$ of u_3 (X_1, X_2, S) evaluated at ($X_1 = 0$, $X_2 = 0$, S), that is

$$w_{r_1r_2}(S) = \left.\frac{\partial^{|r|}u_3}{\partial X_1^{r1}\partial X_2^{r2}}\right|_{(X_1=0,X_2=0,S)} \quad (2)$$

Said a and b two integers greater than or equal to 2, we let the indices r_1 and r_2 in Eqs. (1) and (2) range over {0, 1, …, a} and {0, 1, …, b}, respectively, in such a way that it results $2 \leqslant |r| \leqslant c$, where $c = \sup\{a, b\}$. Throughout the paper, we refer to the following axial component of the displacement field (1)

$$w = \sum_{\substack{r_1 = 0\ldots,a \\ 2 \leqslant |r| \leqslant c}} \sum_{r_2 = 0,\ldots,b} w_{r_1r_2}X_1^{r1}X_2^{r2} \quad (3)$$

as the warping function of the beam cross-sections. We also make use of the following power series expansion of $\mathbf{R}(S)$

$$\mathbf{R}(S) = \mathbf{I} + \mathbf{\Phi}(S) + \frac{1}{2!}\mathbf{\Phi}^2(S) + \frac{1}{3!}\mathbf{\Phi}^3(S) + \cdots \quad (4)$$

$\mathbf{\Phi}(S)$ denoting a skew tensor [35]. The displacement field (1) is completely characterized by the generalized displacements given by

$$\hat{\mathbf{u}} = \{v_1, v_2, v_3, \varphi_1, \varphi_2, \varphi_3, w_{20}, w_{11}, w_{02}, \ldots, w_{a0}, \ldots, w_{0b}\} \quad (5)$$

where v_1, v_2, v_3 denote the Cartesian components of $\mathbf{v}$; φ_1, φ_2, φ_3 denote the Cartesian components of the axial vector $\boldsymbol{\varphi}$ of $\mathbf{\Phi}$; and w_{20}, w_{11}, w_{02}, …, w_{a0}, …, w_{0b} denote the coefficients appearing in the warping function (3) (we have here dropped the dependence on S of the generalized displacements, for the sake of simplicity). We let m_w denote the number of warping coefficients (corresponding to the particular choice made for a and b), and $m = 6 + m_w$ the total number of the generalized displacements characterizing the present model.

On the basis of the above assumptions, a moderate rotation theory of laminated curved beams has been fully developed in [35], to which we refer the reader for the details. We will illustrate some of the main features of such a theory in the following sections.

3. Finite element model

Let C^h denote a finite-element discretization of the beam axis into a collection of four-nodes Lagrangian elements $C_1, \ldots, C_{n_e}$ (Fig. 1)

$$C^h = \bigcup_{e=1}^{n_e} C_e \quad (6)$$

On adopting isoparametric elements, we use the same shape functions to approximate both the geometry and the displacement field over the generic finite element C_e, that is

$$Z_{2_e}^h = \sum_{I=1}^{n} N_I Z_{2_I}, \quad Z_{3_e}^h = \sum_{I=1}^{n} N_I Z_{3_I}, \quad \hat{\mathbf{u}}_e^h = \sum_{I=1}^{n} N_I \hat{\mathbf{u}}_I \quad (7)$$

where N_I is the shape function corresponding to node I, which consists of a complete polynomial of order $n-1$; Z_{2_I}, and Z_{3_I} are the Cartesian coordinates of I in the global reference frame {O, Z_1, Z_2, Z_3} (Fig. 1); $\hat{\mathbf{u}}_I$ is the generalized displacement vector relative to node I.

The transformation which maps the straight master element into a curved (cubic) element, is graphically represented in Fig. 2.

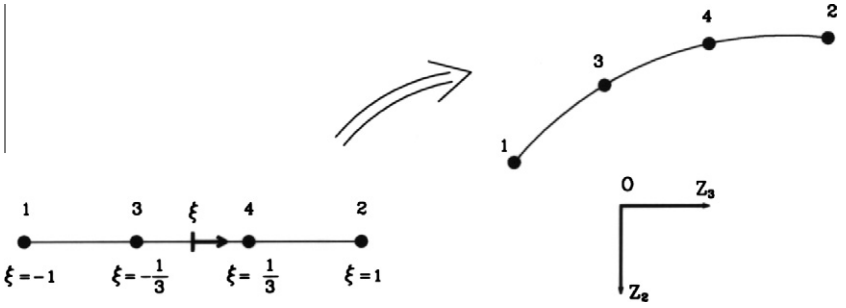

Fig. 2. Transformation of the master element into the current element of the beam axis.

The Jacobian of the transformation from the normalized coordinate ξ (Fig. 2) to the curvilinear abscissa $X_3 = S$ (Fig. 1) is given by [42]

$$J = \frac{dX_3}{d\xi} = \sqrt{\left(\frac{dZ^h_{2_e}}{d\xi}\right)^2 + \left(\frac{dZ^h_{3_e}}{d\xi}\right)^2} = \sqrt{\left(\sum_{I=1}^{n} N_{I,\xi} Z_{2_I}\right)^2 + \left(\sum_{I=1}^{n} N_{I,\xi} Z_{3_I}\right)^2} \tag{8}$$

where $N_{I,\xi}$ is the derivative of N_I with respect to ξ,, and Z_{2_I} and Z_{3_I} are the in-plane Cartesian coordinates of node I (Fig. 2). Consequently, the derivative of N_I with respect to X_3, which we denote by the apex $'$, may be written as follows:

$$N'_I = \frac{dN_I}{dX_3} = J^{-1} N_{1,\xi} \tag{9}$$

Let now $M = 4m$ denote the total number of generalized displacements that characterize the kinematics of the generic finite element C_e. It is convenient to rewrite $(7)_3$ into the following matrix form:

$$\hat{\mathbf{u}}^h_e = \mathbf{N}\mathbf{U}_e \tag{10}$$

where $\mathbf{U}_e$ is the M-dimensional vector collecting all the generalized displacements of $C_e\left(\mathbf{U}_e = \left[\hat{\mathbf{u}}^T_1, \hat{\mathbf{u}}^T_2, \ldots, \hat{\mathbf{u}}^T_n\right]^T\right)$, while $\mathbf{N}$ is the following matrix:

$$\mathbf{N}_{[n\times M]} = [\mathbf{N_1}, \mathbf{N_2}, \ldots, \mathbf{N_n}] \tag{11}$$

with

$$\mathbf{N}_{I[m\times M]} = diag(N_I N_I \ldots N_I) \tag{12}$$

Starting with the approximation (10) of the element (generalized) displacement vector $\hat{\mathbf{u}}^h_e$, we are led to the following approximation of the σ-dimensional vector of the generalized strains of C_e ($\sigma = 9 + 2m_w$, cf. [35]):

$$\widehat{\mathbf{E}}^h_e(\mathbf{U}_e) = \widehat{\mathbf{E}}^{(1)h}_e(\mathbf{U}_e) + \frac{1}{2}\widehat{\mathbf{E}}^{(2)h}_e(\mathbf{U}_e, \mathbf{U}_e) \tag{13}$$

where

$$\widehat{\mathbf{E}}^{(1)h}_e(\mathbf{U}_e) = \mathbf{B}_0\mathbf{U}_e, \quad \widehat{\mathbf{E}}^{(2)h}_e(\mathbf{U}_e, \delta\mathbf{U}_e) = \mathbf{B}_L(\mathbf{U}_e)\delta\mathbf{U}_e \tag{14}$$

Here, $\mathbf{B}_0$ and $\mathbf{B}_L(\mathbf{U}_e)$ are the following $\sigma \times M$ matrices:

$$\mathbf{B} = [\mathbf{B}_{0_1}, \mathbf{B}_{0_2}, \ldots \mathbf{B}_{0_n}], \quad \mathbf{B}_L(\mathbf{U}_e) = \mathbf{A}(\mathbf{U}_e)\mathbf{G} \tag{15}$$

with the $\sigma \times m$ submatrices $\mathbf{B}_{0_I}$ defined through:

$$\mathbf{B}_{0_I} = \begin{bmatrix} \mathbf{B}^{Ev}_{0_I} & \mathbf{B}^{E\phi}_{0_I} & 0 \\ 0 & \mathbf{B}^{\Theta\phi}_{0_I} & 0 \\ 0 & 0 & 0 \\ 0 & 0 & \mathbf{B}^{ww}_{0_I} \\ 0 & 0 & \mathbf{B}^{w'w'}_{0_I} \end{bmatrix} \tag{16}$$

where

$$\mathbf{B}^{EV}_{0_I} = \mathbf{B}^{\Theta\phi}_{0_I} = \begin{bmatrix} N'_1 & 0 & 0 \\ 0 & N'_1 & N_I/R \\ 0 & -N_I/R & N'_1 \end{bmatrix}, \quad \mathbf{B}^{E\phi}_{0_I} = \begin{bmatrix} 0 & -N'_1 & 0 \\ N_I & 0 & 0 \\ 0 & 0 & 0 \end{bmatrix}$$

$$\mathbf{B}^{ww}_{0_I\ [m_w\times m_w]} = diag(N_I N_I \ldots N_I),$$
$$\mathbf{B}^{w'w'}_{0_I\ [m_w\times m_w]} = diag(N'_I N'_I \ldots N'_I) \tag{17}$$

The $\mathbf{A}$ and $\mathbf{G}$ matrices appearing in Eq. $(15)_2$ are instead given by:

$$\mathbf{A}(\mathbf{U}_e)_{[\sigma\times m]} = \begin{bmatrix} \mathbf{A}(\mathbf{U}_e) \\ \mathbf{0} \end{bmatrix}, \quad \mathbf{G}_{[9\times M]} = [\mathbf{G}_1, \mathbf{G}_2, \ldots, \mathbf{G}_n] \tag{18}$$

where

$$\mathbf{G}_{I[9\times m]} = [\overline{\mathbf{G}}_I, \mathbf{0}], \quad \overline{\mathbf{G}}_{I[9\times 6]} = \begin{bmatrix} N'_I & 0 & 0 & 0 & 0 & 0 \\ 0 & N'_I & 0 & 0 & 0 & 0 \\ 0 & 0 & N_I & 0 & 0 & 0 \\ 0 & 0 & 0 & N_I & 0 & 0 \\ 0 & 0 & 0 & 0 & N_I & 0 \\ 0 & 0 & 0 & 0 & 0 & N_I \\ 0 & 0 & 0 & N'_I & 0 & 0 \\ 0 & 0 & 0 & 0 & N'_I & 0 \\ 0 & 0 & 0 & 0 & 0 & N'_I \end{bmatrix} \tag{19}$$

$$\overline{\mathbf{A}}(\mathbf{U_e})_{[9\times 9]} = \begin{bmatrix} 0 & \phi_3 & \frac{\phi_3}{R} & \frac{\phi_3}{2} & 0 & \left(v'_2 - \frac{v_3}{R} - \frac{\phi_1}{2}\right) & 0 & 0 & 0 \\ -\phi_3 & 0 & 0 & 0 & \frac{\phi_3}{2} & \left(-v'_I + \frac{\phi_2}{2}\right) & 0 & 0 & 0 \\ v'_1 & \left(v'_2 + \frac{v_3}{R}\right) & \left(\frac{v'_2}{R} + \frac{v_3}{R^2}\right) & 0 & 0 & 0 & 0 & 0 & 0 \\ \left(-\phi'_3 + \frac{\phi_2}{R}\right) & 0 & 0 & 0 & \left(\frac{v'_I}{R} - \frac{\phi_2}{R} + \frac{\phi'_3}{2}\right) & \left(\frac{\phi'_2}{2} + \frac{\phi_3}{R}\right) & 0 & \frac{\phi_3}{2} & \left(-v'_I + \frac{\phi_2}{2}\right) \\ 0 & \left(-\phi'_3 + \frac{\phi_2}{R}\right) & \left(-\frac{\phi'_3}{R} + \frac{\phi_2}{R^2}\right) & \left(-\frac{\phi'_2}{2} + \frac{\phi_2}{2R}\right) & \left(\frac{v'_2}{R} + \frac{v_3}{R^2} + \frac{\phi_1}{2R}\right) & -\frac{\phi'_I}{2} & -\frac{\phi_3}{2} & 0 & \left(-v'_2 - \frac{v_3}{R} - \frac{\phi_1}{2}\right) \\ 0 & 0 & 0 & \left(-\frac{\phi'_2}{2} - \frac{\phi_3}{2R}\right) & \frac{\phi'_I}{2} & -\frac{\phi_I}{2R} & \frac{\phi_2}{2} & -\frac{\phi_I}{2} & 0 \\ 0 & 0 & 0 & 0 & \left(-\frac{\phi'_3}{R} + \frac{\phi_2}{R^2}\right) & \left(\frac{\phi'_2}{R} + \frac{\phi_3}{R^2}\right) & 0 & \left(-\phi'_3 + \frac{\phi_3}{R}\right) & \left(-\phi'_3 + \frac{\phi_2}{R}\right) \\ 0 & 0 & 0 & 0 & \left(-\frac{\phi'_3}{R} + \frac{\phi_2}{R^2}\right) & 0 & \phi'_I & 0 & \left(-\phi'_3 + \frac{\phi_2}{R}\right) \\ 0 & 0 & 0 & 0 & 0 & \frac{\phi'_I}{R} & \left(-\phi'_2 + \frac{\phi_3}{R}\right) & \phi'_1 & 0 \end{bmatrix} \tag{20}$$

3.1. Branch switching procedure

The potential energy of the present beam model is given by:

$$\begin{aligned}\Pi(\hat{\mathbf{u}};\lambda) = &\frac{1}{2}\\ &\times \int_0^L \left[\widehat{\mathbf{E}}^{(1)}(\hat{\mathbf{u}}) + \frac{1}{2}\widehat{\mathbf{E}}^{(2)}(\hat{\mathbf{u}},\hat{\mathbf{u}})\right]^T \widehat{\mathbf{D}} \left[\widehat{\mathbf{E}}^{(1)}(\hat{\mathbf{u}}) + \frac{1}{2}\widehat{\mathbf{E}}(\hat{\mathbf{u}},\hat{\mathbf{u}})\right] dS\\ &- \lambda \int_0^L \hat{\mathbf{u}}^T \left[\hat{\mathbf{q}}^{(1)} + \frac{1}{2}\hat{\mathbf{q}}^{(2)}(\hat{\mathbf{u}})\right] dS\\ &+ -\lambda \hat{\mathbf{u}}(0)^T \left[\widehat{\mathbf{Q}}_0^{(1)} + \frac{1}{2}\widehat{\mathbf{Q}}_0^{(2)}(\hat{\mathbf{u}}(0))\right]\\ &- \lambda \hat{\mathbf{u}}(L)^T \left[\widehat{\mathbf{Q}}_l^{(1)} + \frac{1}{2}\widehat{\mathbf{Q}}_l^{(2)}(\hat{\mathbf{u}}(L))\right]\end{aligned} \tag{21}$$

where $\widehat{\mathbf{D}}$ denotes the $\sigma \times \sigma$ generalized elasticity matrix; λ denotes a multiplier of the external loads; $\hat{\mathbf{q}}$ and $\hat{\mathbf{q}}^{(2)}(\hat{\mathbf{u}})$ denote the first-order and second-order generalized forces per unit length, respectively; and $\widehat{\mathbf{Q}}_0^{(1)}$, $\widehat{\mathbf{Q}}_l^{(1)}$ and $\widehat{\mathbf{Q}}_0^{(2)}(\hat{\mathbf{u}}(0))$, $\widehat{\mathbf{Q}}_l^{(2)}(\hat{\mathbf{u}}(L))$ denote the first-order and second-order generalized forces acting on the bases of the beam, respectively (check Ref. [35] for further details). We here generalize the expression of $\widehat{\mathbf{D}}$ given in [35], in order to account for bimodular response of the composite material that forms the beam. This is obtained by introducing the following expressions of the local elastic moduli, which appear in the expression of $\widehat{\mathbf{D}}$ provided in Appendix A

$$Q_{ij} = [1 - H(E_{3'3'})]Q_{ij}^- + H(E_{3'3'})Q_{ij}^+ \tag{22}$$

Here, $E_{3'3'}$ is the component of the Green-Saint Venant strain tensor in the direction of the fibers forming the composite material ($3'$ axis); Q_{ij}^+ are the elastic moduli of the material when such fibers are elongated ($E_{3'3'} > 0$); Q_{ij}^- are the elastic moduli when the same fibers are instead shortened ($E_{3'3'} < 0$)); and $H(E_{3'3'})$ is the Heaviside function

$$H(E_{3'3'}) = \begin{cases} 0, & \text{if } E_{3'3'} < 0 \\ 1, & \text{if } E_{3'3'} \geqslant 0 \end{cases} \tag{23}$$

Let us now denote the finite element approximation of the potential energy (21) by $\Pi^h(\mathbf{U},\lambda)$, where $\mathbf{U}$ indicates the overall (global) generalized displacement vector. We write the equilibrium equations of the present finite element model into the following variational form:

$$\delta\Pi^h = \delta\mathbf{U}^T\mathbf{R}(\mathbf{U},\lambda) \tag{24}$$

where $\delta\Pi^h$ is the first variation of Π^h with increment $\delta\mathbf{U}$; and $\mathbf{R}(\mathbf{U},\lambda)$ (residual vector) is the derivative of Π^h with respect to $\mathbf{U}$. Eqs. (10), (13) and (14) of the previous section allow us to rewrite (24) as follows:

$$\delta\mathbf{U}^T\mathbf{R}(\mathbf{U},\lambda) = \delta\mathbf{U}^T\{\mathbf{K}(\mathbf{U})\mathbf{U} - \lambda[\mathbf{Q}^{(1)} + \mathbf{Q}^{(2)}(\mathbf{U})]\} = 0 \tag{25}$$

where $\mathbf{K}(\mathbf{U})$ is the $N \times N$ global stiffness matrix, N denoting the total number of degrees of freedom of the overall finite element model, while $\mathbf{Q}^{(1)}(\mathbf{U})$, $\mathbf{Q}^{(2)}(\mathbf{U})$ are the global force vectors, which derive from the assembly of the element vectors

$$\mathbf{Q}_e^{(1)} = \int_{-1}^{1} \mathbf{N}^T\hat{\mathbf{q}}_e^{(1)} J d\xi, \quad \mathbf{Q}_e^{(2)}(\mathbf{U}_e) = \int_{-1}^{1} \mathbf{N}^T\hat{\mathbf{q}}_e^{(2)}(\mathbf{U}_e) J d\xi \tag{26}$$

and the nodal force vectors $\widehat{\mathbf{Q}}_e^{(1)}(\hat{\mathbf{u}}_\mathbf{I})$, $\widehat{\mathbf{Q}}_e^{(2)}(\hat{\mathbf{u}}_\mathbf{I})$ $(I = 1,2,\ldots,n_n)$. The global stiffness matrix $\mathbf{K}(\mathbf{U})$ is obtained by assembling the following element matrices $\mathbf{K}_e (e = 1, 2, \ldots, n_e)$

$$\mathbf{K}_e(\mathbf{U}_e) = \int_{-1}^{1} \left[\mathbf{B}_0^T + \mathbf{B}_L^T(\mathbf{U}_e)\right]\widehat{\mathbf{S}}(\mathbf{U}_e) J d\xi \tag{27}$$

with $\widehat{\mathbf{S}}$ denoting the generalized stress vector defined through

$$\widehat{\mathbf{S}}(U_e) = \widehat{\mathbf{D}}\left[\mathbf{B}_0 + \frac{1}{2}\mathbf{B}_L(\mathbf{U}_e)\right]U_e \tag{28}$$

Due to the arbitrariness of $\delta\mathbf{U}$, Eq. (25) is equivalent to the following nonlinear system of N equations

$$\mathbf{R}(\mathbf{U},\lambda) = \mathbf{K}(\mathbf{U})\mathbf{U} - \lambda[\mathbf{Q}^{(1)} + \mathbf{Q}^{(2)}(\mathbf{U})] \tag{29}$$

that can be solved through the path-following procedure provided in [35], in order to follow an arbitrary equilibrium path of the finite element model at hand. We say that a couple $\mathbf{U}$, λ is a stability point of a given equilibrium path if there exist some nonzero $\mathbf{V}$ (buckling mode) that solves the following variational equation [43]

$$D_U^2\Pi_e^h(\mathbf{U},\lambda)\mathbf{V}\delta\mathbf{U} = \delta\mathbf{U}^T\mathbf{K}_T(\mathbf{U},\lambda)\mathbf{V} = 0 \tag{30}$$

for each variation $\delta\mathbf{U}$ of the global displacement vector $\mathbf{U}$. Eq. (30) is equivalent to the following system of N algebraic equations

$$\mathbf{K}_T(\mathbf{U},\lambda)\mathbf{V} = \mathbf{0} \tag{31}$$

where $\mathbf{K}_T$ is the tangent stiffness matrix provided in Appendix B. In order to exclude the trivial case $\mathbf{V} = \mathbf{0}$, we append the following constraint equation

$$\mathbf{e}_p^T\mathbf{V} - V_0 = 0 \tag{32}$$

to (31), with V_o being a given value of the pth component of $\mathbf{V}$. After reducing $\mathbf{K}_T$ to an upper triangular matrix (by Gauss elimination), we identify the index p in (32) with the entry of the lowest diagonal term of the reduced stiffness matrix. Concerning $\boldsymbol{V}_0$, we set

$$V_0 = \frac{\mathbf{e}_p^T\mathbf{V}_0}{\|\mathbf{V}_0\|} \tag{33}$$

with $\mathbf{V}_0$ being the initial approximation to $\mathbf{V}$.

We classify stability points into limit (or turning) and bifurcation points according to the following criterion [37,38]

$$\textit{Bifurcation Point}: \quad \mathbf{V}^T(\mathbf{Q}^{(1)} + \mathbf{Q}^{(2)}(\mathbf{U})) = \mathbf{0} \tag{34}$$

$$\textit{Limit Point}: \quad \mathbf{V}^T(\mathbf{Q}^{(1)} + \mathbf{Q}^{(2)}(\mathbf{U})) \neq \mathbf{0} \tag{35}$$

An efficient procedure for the computation of stability points of finite element models has been proposed by Simo and Wriggers in [38]. It consists of solving the extended system:

$$\mathbf{R}^{**}(\mathbf{U},\mathbf{V},\lambda,\mu) = \begin{Bmatrix} \mathbf{R}(\mathbf{U},\lambda) \\ \mathbf{K}_T(\mathbf{U},\lambda)\mathbf{V} \\ \mathbf{e}_p^T\mathbf{V} - \boldsymbol{V}_0 \\ \mathbf{e}_p^T\mathbf{U} - \mu \end{Bmatrix} = \mathbf{0} \tag{36}$$

which derives from the addition of Eqs. (31) and (32) to (29).

Since the tangent stiffness matrix becomes ill-conditioned as the solution of (36) approaches a stability point, it is convenient to transform the extended system (36) into the following equivalent form [38]

$$\mathbf{R}^{**}(\mathbf{U},\mathbf{V},\lambda,\mu) = \begin{Bmatrix} \mathbf{R}(\mathbf{U},\lambda) + \eta(\mathbf{e}_p^T\mathbf{U} - \mu)\mathbf{e}_p \\ \mathbf{K}_T(\mathbf{U},\lambda)\mathbf{V} + \eta(\mathbf{e}_p^T\mathbf{V} - \mathbf{V}_0)\mathbf{e}_p \\ \mathbf{e}_p^T\mathbf{V} - \boldsymbol{V}_0 \\ \mathbf{e}_p^T\mathbf{U} - \boldsymbol{\mu} \end{Bmatrix} = 0 \tag{37}$$

with η being an arbitrary positive number. The Newton–Raphson linearization of (37) leads to obtain the incremental equations

$$\begin{bmatrix} \mathbf{K}_{T_\eta} & \mathbf{0} & -\mathbf{Q} & -\eta\mathbf{e}_p \\ D_U(\mathbf{K}_T\mathbf{V}) & \mathbf{K}_{T_\eta} & D_\lambda(\mathbf{K}_T\mathbf{V}) & \mathbf{0} \\ \mathbf{0} & \mathbf{e}_p^T & 0 & 0 \\ \mathbf{e}_p^T & \mathbf{0} & 0 & -1 \end{bmatrix} \begin{Bmatrix} \Delta\mathbf{U} \\ \Delta\mathbf{V} \\ \Delta\lambda \\ \Delta\mu \end{Bmatrix} = \begin{Bmatrix} \mathbf{R}(\mathbf{U},\lambda) + \eta\left(\mathbf{e}_p^T\mathbf{U} - \mu\right)\mathbf{e}_p \\ \mathbf{K}_T(\mathbf{U},\lambda)\mathbf{V} - (\eta V_0)\mathbf{e}_p \\ \mathbf{e}_p^T\mathbf{V} - V_0 \\ \mathbf{e}_p^T\mathbf{U} - \mu \end{Bmatrix} \tag{38}$$

where

$$\mathbf{Q} = \mathbf{Q}^{(1)} + \mathbf{Q}^{(2)}(\mathbf{U}) \tag{39}$$

$$\mathbf{K}_{T_\eta}(\mathbf{U},\lambda) = \mathbf{K}_T(\mathbf{U},\lambda) + \eta\mathbf{e}_p\mathbf{e}_p^T \ (p \text{ not summed}) \tag{40}$$

The nonsymmetric system (38) can be approached through the following bordering algorithm [29], where *TOL* denotes a prescribed (dimensionless) tolerance.

1. *Assume a predictor* $\widetilde{\mathbf{U}},\ \widetilde{\mathbf{V}},\ \tilde{\lambda},\ \tilde{\mu}$ and evaluate

$$\widetilde{\mathbf{R}} = \mathbf{R}(\widetilde{\mathbf{U}},\tilde{\lambda}), \quad \widetilde{\mathbf{K}}_{T_\eta} = \mathbf{K}_{T_\eta}(\widetilde{\mathbf{U}},\tilde{\lambda}), \quad \widetilde{\mathbf{Q}}^{(2)} = \mathbf{Q}^{(2)}(\widetilde{\mathbf{U}}) \tag{41}$$

2. *Compute the partial solutions from* $(38)_1$

$$\begin{aligned} \Delta\mathbf{U}_1 &= \widetilde{\mathbf{K}}_{T_\eta}^{-1}(\mathbf{Q}^{(1)} + \widetilde{\mathbf{Q}}^{(2)}) \\ \Delta\mathbf{U}_2 &= -\widetilde{\mathbf{K}}_{T_\eta}^{-1}\widetilde{\mathbf{R}} \\ \Delta\mathbf{U}_3 &= -\widetilde{\mathbf{K}}_{T_\eta}^{-1}\mathbf{e}_p \end{aligned} \tag{42}$$

3. *Compute the partial solutions from* $(38)_2$

$$\begin{aligned} \mathbf{q}_1 &= \widetilde{\mathbf{K}}_{T_\eta}^{-1}\mathbf{h}_1 \\ \mathbf{q}_2 &= \widetilde{\mathbf{K}}_{T_\eta}^{-1}\mathbf{h}_2 \\ \mathbf{q}_3 &= \widetilde{\mathbf{K}}_{T_\eta}^{-1}\mathbf{h}_3 \\ \mathbf{q}_4 &= \widetilde{\mathbf{K}}_{T_\eta}^{-1}\mathbf{h}_4 \end{aligned} \tag{43}$$

where

$$\begin{aligned} \mathbf{h}_1 &= D_U(\mathbf{K}_T\mathbf{V})\Delta U_1 \\ \mathbf{h}_2 &= D_U(\mathbf{K}_T\mathbf{V})\Delta U_2 \\ \mathbf{h}_3 &= D_U(\mathbf{K}_T\mathbf{V})\Delta U_3 \\ \mathbf{h}_4 &= D_\lambda(\mathbf{K}_T\mathbf{V}) \end{aligned} \tag{44}$$

4. *Compute* $\Delta\lambda$ *and* $\Delta\mu$*.The increments* $\Delta\lambda$ *and* $\Delta\mu$ *can be computed from Eq.* $(38)_{3-4}$*, which can be written as*

$$\begin{bmatrix} \mathbf{e}_p^T(\mathbf{q}_1 + \mathbf{q}_4) & \eta\mathbf{e}_p^T\mathbf{q}_3 \\ \mathbf{e}_p^T\Delta\mathbf{U}_1 & (\eta\mathbf{e}_p^T\Delta\mathbf{U}_3 - 1) \end{bmatrix} \begin{Bmatrix} \Delta\lambda \\ \Delta\mu \end{Bmatrix} = \begin{Bmatrix} g_1 \\ g_2 \end{Bmatrix} \tag{45}$$

where

$$\begin{aligned} g_1 &= V_0 - \mathbf{e}_p^T[\mathbf{q}_2 + \eta V_0\Delta\mathbf{U}_3 + \eta(\mu - \mathbf{e}_p^T\widetilde{\mathbf{U}})\mathbf{q}_3] \\ g_2 &= \mu - \mathbf{e}_p^T[\widetilde{\mathbf{U}} + \Delta\mathbf{U}_2 + \eta(\mu - \mathbf{e}_p^T\widetilde{\mathbf{U}})\Delta\mathbf{U}_3] \end{aligned} \tag{46}$$

5. *Compute* $\Delta\mathbf{U}$ *and* $\Delta\mathbf{V}$ *from the equations*

$$\begin{aligned} \Delta\mathbf{U} &= \Delta\lambda\Delta\mathbf{U}_1 + \Delta\mathbf{U}_2 + \eta\left(\mu\Delta\mu - \mathbf{e}_p^T\widetilde{\mathbf{U}}\right)\Delta\mathbf{U}_3 \\ \Delta\mathbf{V} &= -\widetilde{\mathbf{V}} + \Delta\lambda(\mathbf{q}_1 + \mathbf{q}_4) + \mathbf{q}_2 + \eta\left[\left(\mu + \Delta\mu - \mathbf{e}_p^T\widetilde{\mathbf{U}}\right)\mathbf{q}_3 + V_0\Delta\mathbf{V}_3\right] \end{aligned} \tag{47}$$

and update: $\mathbf{U} = \widetilde{\mathbf{U}} + \Delta\mathbf{U}, \quad \mathbf{V} = \widetilde{\mathbf{V}} + \Delta\mathbf{V}, \quad \lambda = \tilde{\lambda} + \Delta\lambda, \quad \mu = \tilde{\mu} + \mu.$

6. *If*

$$\frac{\|\mathbf{R}_\mu^{**}(\mathbf{U},\mathbf{V},\lambda,\mu)\|}{\|\lambda(\mathbf{Q}^{(1)} + \mathbf{Q}^{(2)}(\mathbf{U}))\|} \leqslant TOL \tag{48}$$

Then stop. Else Go To 2 and set $\widetilde{\mathbf{U}} = \mathbf{U}, \quad \widetilde{\mathbf{V}} = \mathbf{V}, \quad \lambda = \lambda, \quad \tilde{\mu} = \mu.$

The expressions of the vectors $\mathbf{h}_j$ ($j = 1, \ldots, 4$) appearing in Eq. (44) are provided in Appendix B.

In correspondence with each point of a given equilibrium path, we check the sign of the determinant of the tangent stiffness matrix, which is a relatively simple operation, since the path-following procedure here used to solve the equilibrium problem (29) requires the factorization of $\mathbf{K}_T$ [35]. If the sign of det ($\mathbf{K}_T$) changes between two successive equilibrium states, say the ith and the $i+1$th ones, we enter the above bordering algorithm on assuming $\widetilde{\mathbf{U}} = \mathbf{U}^{i+1},\ \tilde{\lambda} = \lambda^{i+1},\ \tilde{\mu} = \mathbf{e}_p^T\mathbf{U}^{i-1},\ \widetilde{\mathbf{V}} = \mathbf{V}_0 = \mathbf{K}_0^{-1}\mathbf{e}_p$ as first predictor. Once a stability point $\mathbf{U}_c$, λ_c has been computed, we detect if it as a limit or a bifurcation point, according to (34) and (35). In the case of a limit point, we switch back to the path-following procedure to complete the primary equilibrium path. In the case of a bifurcation point, we instead switch the path-following procedure to the secondary (or bifurcated) path, by adding a vector proportional to the eigenvector $\mathbf{V}$ to the stability point $\mathbf{U}_c$ [35]. We arrest the calculations when the cross-section rotations and/or the shear strains of the examined model are more than moderately large, or the axial strains are no longer infinitesimally small.

4. Numerical results

We present in this section some numerical results dealing with the stability points and the post-buckling behavior of illustrative examples of straight and curved beams. We start presenting some results concerned with unimodular beams (same behavior in tension and compression), which aim to show the accuracy of the present model, by way of comparison to classical beam theories. Next, we present some original results concerned with the stability of bimodular composite beams.

In all the examined examples, we assume that beam cross-section is rectangular with dimension H_1 and H_2 along the directions X_1 and X_2, respectively. We denote the cross-section area by $A = H_1H_2$; the moments of inertia by I_1 and I_2; the polar moment of inertia by I_G and the De Saint Venant torsional rigidity by J_t

$$I_1 = \frac{1}{12}H_1H_2^3, \quad I_2 = \frac{1}{12}H_1^3H_2, \quad I_G = I_1 + I_2, \quad J_t = \frac{1}{3}H_1^3H_2 \tag{49}$$

Concerning the warping function w, we examine the following cases

- No Warping (NW): $w = 0$.
- W1 Warping Function: $w = w_{11}X_1X_2$.
- W3 Warping Function: $w = w_{20}X_1^2 + w_{11}X_1X_2 + w_{02}X_2^2 + w_{30}X_1^3 + w_{21}X_1^2X_2 + w_{12}X_1X_2^3 + w_{03}X_2^3$.

We make use of a four point Gauss quadrature formula to compute the tangent stiffness matrix, and its derivatives. In the case of a bimodular material, we also use a Gauss quadrature formula to numerically integrate the generalized elasticity matrix of each lamina of the beam (cf. Section 3.1).

4.1. Buckling of unimodular beams

The first results that we present are concerned with the lateral buckling of straight and curved beams featuring isotropic unimodular material (Poisson's ratio equal to 0.3).

We start analyzing the lateral buckling of a moderately deep, simply supported beam transversally loaded at the mid-span ($H_1/H_2 = 0.1$, $L/H_2 = 10$). Three different load conditions are considered: load at the centroid; load at the extrados ($X_1 = 0$, $X_2 = -H_2/2$): and load at the intrados ($X_1 = 0$, $X_2 = +H_2/2$). It is easy to show the last two cases give rise to deformation-dependent loading ($\mathbf{Q}^{(2)}(\mathbf{U}) \neq \mathbf{0}$).

Table 1 shows a comparison between the bifurcation points computed through the present theory (PT) and those corresponding to classical Prandtl's theory (CT, see, e.g., [39]). The PT-results were computed through a bilinear warping function (W1), assuming either geometrically nonlinear pre-buckling behavior (NLPB),

Table 1
Lateral buckling of a deep simply supported beam loaded by a transverse force Q at the mid-span ($H_1/H_2 = 0.1$, $L/H_2 = 10$, 20 finite elements).

	CT-LPB	PT-LPB	CT-NLPB	PT-NLPB
Load at the centroid				
$v_M/L \times 100$	0.4380	0.4483	0.4401	0.4520
λ_{Bif}	16.940	16.902	17.020	17.040
Load at the extrados				
$v_M/L \times 100$	0.4053	0.4152	0.4071	0.4183
λ_{Bif}	15.752	15.654	15.745	15.772
Load at the intrados				
$v_M/L \times 100$	0.4656	0.4832	0.4743	0.4874
λ_{Bif}	18.127	18.215	18.346	18.376
CT: Classical Theory		LPB: Linear Pre-Buckling		
PT: Present Theory		NLPB: Nonlinear Pre-Buckling		
v_M: mid span in-plane displacement		$\lambda_{Bif} = Q_{Bif}/\left(\sqrt{EI_2 GJ_t}/L^2\right)$		

Table 2
Lateral buckling of a hinged semicircular arch and a clamped semicircular arch subject to uniformly distributed dead load q along the centerline ($H_1/H_2 = 0.1$, $L/H_2 = 10$, 20 finite elements).

	$\lambda_{Bif} = q_{Bif}/\left(\sqrt{EI_2}/R^3\right)$	
	Classical theory	Present theory
Hinged arch	1.9358	1.9361
Clamped arch	13.514	13.774

or linear pre-buckling behavior (LPB). The first case is analyzed through the present finite element model, while the second one corresponds to a simplified version of such a model, obtained by discarding the part $\mathbf{K}_L$ of the tangent stiffness matrix (cf. Appendix B). In the NLPB case, we suitably generalize the original Prandtl's theory, by using the present model, neglecting shear deformation, warping-and quadratic-terms of the axial strain field [35], and assuming torsional stiffness equal to GI_G. The results in Table 1 highlight the PT very well agrees with the CT in all the examined cases.

We now pass to study the lateral buckling of moderately deep semicircular arches that are either hinged or clamped at the ends. The loading condition consists of a uniform radial dead load along the centerline. Table 2 shows that the results of the present theory (W1 warping model) are in good agreement with those obtained in [39] (through the classical beam theory) in each of the above cases.

Next, we study the snap-through buckling of a shallow circular arch clamped at the ends and carrying a central point load, which has been studied by Dawe in Ref. [40] through Marguerre's shallow arch theory. The analyzed arch has a base length of 863.6 mm, a central rise of 27.69 mm and a cross-section with width of 25.4 mm (H_1) and thickness of 4.76 mm (H_2). The material is isotropic with Young's modulus $E = 72{,}395$ N/mm^2. We show the load vs. central deflection and load vs. axial thrust curves obtained through the present model and Dawe's theory in Figs. 3 and 4. It is seen that such theories are in rather good agreement each other.

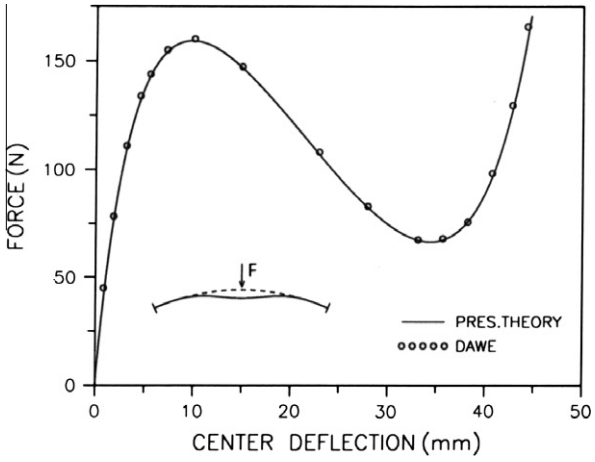

Fig. 3. Load-central deflection curve of a clamped shallow arch carrying a central point force.

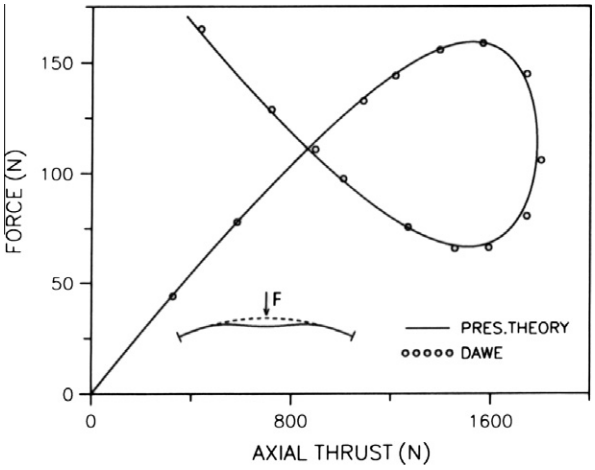

Fig. 4. Load-axial thrust curve of a clamped shallow arch carrying a central point force.

4.2. Buckling of bimodular beams

The present section deals with the buckling and post-buckling behavior of straight beams and laminated arches made up of bimodular materials.

First, we consider the buckling problem of an axially loaded simply supported beam made up of an isotropic bimodular material ($H_1/H_2 = 1$, $L/H_2 = 10$), using a Gauss quadrature formula with 12 points over the beam thickness to compute the (generalized) elasticity matrix. Fig. 5 shows the load vs. center deflection curves that we obtain through the present model for several values of the ratio between the Young modulus characterizing the material response in compression E^-, and the analogous modulus in tension E^+ ($m = E^-/E^+$ bimodularity ratio). The present results are compared with those obtained in Bruno et al. [41] through an "imperfect" beam model showing an initial deflection equal to 1% of the beam length.

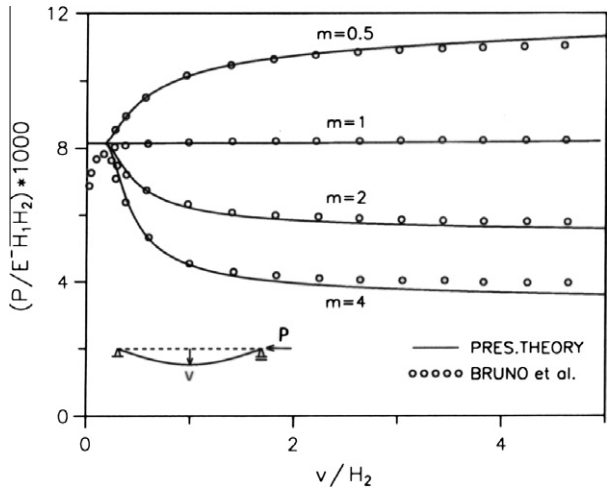

Fig. 5. Load-central deflection curves of axially loaded bimodular beams.

It can be observed that the load–deflection curves in Fig. 5 are not sensitive the bimodularity ratio m before buckling, and in the very initial part of the secondary equilibrium path (close to the buckling point), since in such regions the beam is under uniform or slightly nonuniform compression. As soon as the material "feels" tensile strains and stresses (post-buckling range), the response of the beam instead appears markedly influence by the actual value of m. In particular, the curves corresponding to $m \neq 1$ (effective bimodular behavior) exhibit stable behavior for $m > 1$ (material stiffer in tension than compression), and unstable behavior for $m < 1$ (material stiffer in compression).

The last two examples we study are concerned with in-plane and lateral buckling of laminated semicircular arches, which are hinged at the ends and carry a radial dead load uniformly distributed along the centerline (Fig. 6, $R/H_2 = 10$).

The examined arches have a 0°/90°/90°/0° lamination scheme (Fig. 6) and are formed by the same composite material in each layer, whose elastic properties are given in Table 3. A Gauss quadrature formula with 4×4 points over the cross-section of each layer is employed to compute the elasticity matrix.

We first examine an arch with transverse aspect ratio $H_1/H_2 = 2$, and deal with its in-plane buckling, which represents the first bifurcation point of the fundamental equilibrium path in the present case. Fig. 7 shows the load vs quarter point radial displacement curves obtained for three different bimodularity ratios ($m = 0.5$, 1.0, 2.0), and two alternative warping models (NW and W3). An appreciable influence of warping effects on the buckling load can be observed (7% difference between the buckling loads predicted by the NW and W3 models). This is explained by the considerably large shear deformability of the examined composite, material which exhibits rather small ratios between the shear moduli and the Young modulus in the direction of the fibers (cf. Table 3). As in the previous example, the post-buckling behavior is stable for $m < 1$ (greater stiffness in tension than compression) and unstable for $m > 1$ (greater stiffness in compression).

Next, we consider an arch with a moderately deep cross-section ($H_1/H_2 = 0.1$), and analyze its lateral buckling (first bifurcation point of the fundamental equilibrium path for such an arch), on

Table 3
Elastic moduli of the bimodular material forming the layers of the arch in Fig. 6.

Young's moduli:	$E^+_{3'} = E^-_{3'}/m, \quad E_{1'} = E_{2'} = E^-_{3'}/25$
Shear moduli:	$G_{3'1'} = G_{2'3'} = E^-_{3'}/50, \quad G_{1'2'} = E_{3'}/125$
Poisson's ratios:	$\upsilon_{1'2'} = \upsilon_{1'3'} = \upsilon_{2'3'} = 0.25$

$3'$ fiber direction, m bimodularity ratio

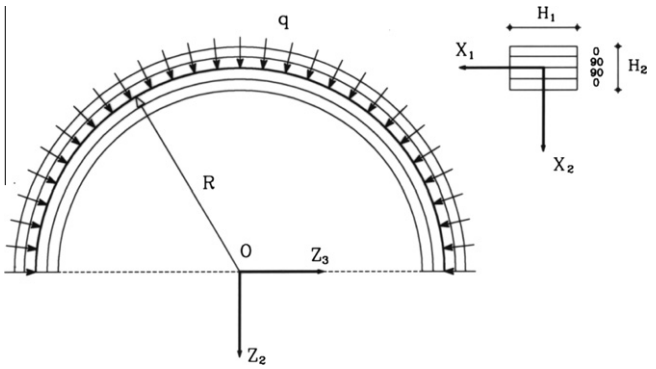

Fig. 6. Loading scheme of a 0°/90°/90°/0° laminated arch featuring bimodular behavior.

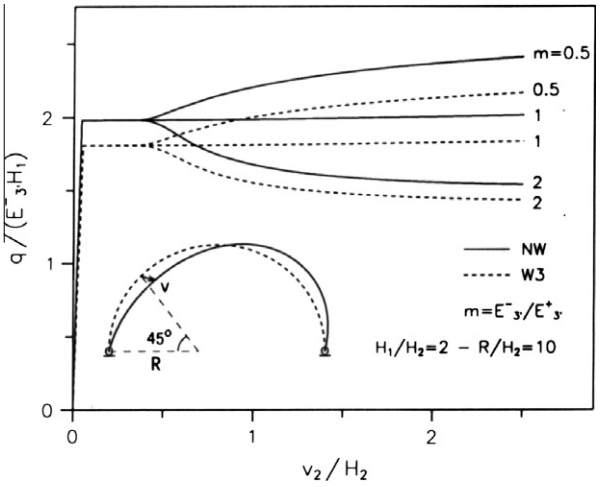

Fig. 7. Load vs. quarter point radial displacement for in-plane buckling of a laminated bimodular arch carrying a uniform radial load q (0/90/90/0 lamination scheme).

considering the warping models W1 and W3 (trivially, it makes no sense to consider the NW model in the present case), and the same bimodularity ratios of the previous example. Fig. 8 shows the load-quarter point lateral displacement curves corresponding to the arch under examination. One can observe that the analyzed

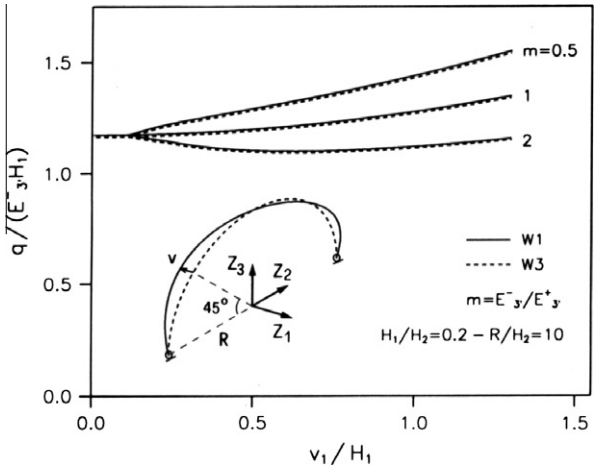

Fig. 8. Load vs. quarter point lateral displacement curves for lateral buckling of a laminated bimodular arch carrying a uniform radial load q (0/90/90/0 lamination scheme).

warping models lead to almost coincident results, which implies that the W1 model is able to accurately describe the problem at hand. The post-buckling response is stable for $m \leqslant 1$. For $m = 2$ the response is instead initially unstable and then progressively turns to stable.

5. Conclusions

We have developed a finite element model that is able to analyze the geometrically nonlinear response, as well as the buckling and post-buckling behaviors of composite curved beams featuring different elastic response in tension and compression. The proposed model is based upon a single-layer formulation of the mechanical theory given in [35], which accounts for warping deformation, moderately large cross-section rotations, moderately-large shear strains, and infinitesimal axial strains in correspondence with the beam axis. Since no assumptions have been made on the magnitude of the beam axis curvature, the given model indifferently applies to straight, shallow and strong curvature beams.

The numerical results provided in Section 4.1 have shown that the present numerical model accurately reduces to classical beam theories in the case of buckling problems of both straight and curved unimodular beams.

We have also presented some numerical results on the buckling and post-buckling responses of straight and curved beams featuring bimodular behavior (Section 4.2). In the straight beam case, the present model has been validated against the model proposed by Bruno et al. in [41], observing an excellent matching between the two analyzed approaches. The results for the curved case have been concerned with the in-plane and out-of-plane buckling of laminated composite arches featuring different ratios between the longitudinal Young modulus (Young modulus in the fiber-direction) in tension and compression. In all the examined problems we have observed that the bimodularity ratio of the material strongly affects the post-buckling behavior of the beam, leading to stable response when the material is stiffer in tension than compression, and unstable (or slightly unstable) response in the opposite case. We have also observed that warping effects play a significant role on the buckling loads of composite beams (for both in-plane and out-of-plane buckling), due to the high shear-deformability of such structures.

The present work paves the way to extensive numerical studies on the bimodular response of straight and curved composite beams subject to different loading and boundary conditions. Another relevant generalization of the current research concerns the extension of the proposed beam model beyond the elastic regime, in order to capture asymmetries in the material response due to different strengths in tension and compression, Additionally, we address a mesh-free formulation of the present model, based on local–global approximating functions selected by maximum entropy [44–46], and/or nonconforming finite element schemes [47], to future work.

Acknowledgments

The authors gratefully acknowledge the support received by Biagio Sciscio (Department of Civil Engineering, University of Salerno) during the course of the present work. FF acknowledges financial support from the University of Salerno through the FARB 2012 grant.

Appendix A

The generalized elasticity matrix of the present model is a square symmetric matrix of size $\sigma \times \sigma$, which can be written in the following partitioned form

$$\widehat{\mathbf{D}} = \begin{bmatrix} \mathbf{D}^{NE} & \mathbf{D}^{N\Theta} & \mathbf{D}^{N\Gamma} & \mathbf{D}^{Nw} & \mathbf{D}^{Nw'} \\ \cdot & \mathbf{D}^{M\Theta} & \mathbf{D}^{M\Gamma} & \mathbf{D}^{Mw} & \mathbf{D}^{Mw'} \\ \cdot & \cdot & \mathbf{D}^{P\Gamma} & \mathbf{D}^{Pw} & \mathbf{D}^{Pw'} \\ \cdot & Sym & \cdot & \mathbf{D}^{vw} & \mathbf{D}^{vw'} \\ \cdot & \cdot & \cdot & \cdot & \mathbf{D}^{w'} \end{bmatrix} \tag{A.1}$$

The following equations provide the expressions of the different submatrices appearing in Eq. (A.1), having denoted the values of the indices r_1 and r_2 corresponding to the kth warping term $w_{r_1 r_2}$ by k_1 and k_2, respectively.

$$\mathbf{D}^{NE} = \begin{bmatrix} \int_\Sigma \frac{Q_{55}}{J} d\Sigma & 0 & \int_\Sigma \frac{Q_{53}}{J} d\Sigma \\ & \int_\Sigma \frac{Q_{44}}{J} d\Sigma & 0 \\ Sym & & \int_\Sigma \frac{Q_{33}}{J} d\Sigma \end{bmatrix} \tag{A.2}$$

$$\mathbf{D}^{N\Theta} = \begin{bmatrix} \int_\Sigma Q_{53} \frac{X_2}{J} d\Sigma & -\int_\Sigma Q_{53} \frac{X_1}{J} d\Sigma & -\int_\Sigma Q_{55} \frac{X_2}{J} d\Sigma \\ 0 & 0 & \int_\Sigma Q_{44} \frac{X_1}{J} d\Sigma \\ \int_\Sigma Q_{33} \frac{X_2}{J} d\Sigma & \int_\Sigma Q_{33} \frac{X_1}{J} d\Sigma & -\int_\Sigma Q_{35} \frac{X_2}{J} d\Sigma \end{bmatrix} \tag{A.3}$$

$$\mathbf{D}^{N\Gamma} = \begin{bmatrix} \int_\Sigma Q_{53} \frac{X_1^2}{J^2} d\Sigma & -\int_\Sigma Q_{53} \frac{X_2^2}{J^2} d\Sigma & -\int_\Sigma Q_{53} \frac{X_1 X_2}{J^2} d\Sigma \\ 0 & 0 & 0 \\ \int_\Sigma Q_{33} \frac{X_1^2}{J^2} d\Sigma & \int_\Sigma Q_{33} \frac{X_2^2}{J^2} d\Sigma & -\int_\Sigma Q_{33} \frac{X_1 X_2}{J^2} d\Sigma \end{bmatrix} \tag{A.4}$$

$$\mathbf{D}^{Nw} = \left[D_{ik}^{Nw} \right] \quad i = 1,2,3; \quad k = 1,2,\ldots,m_w$$

$$\begin{aligned} D_{1k}^{Nw} &= \int_\Sigma k_1 Q_{55} X_1^{K_1 - 1} X_2^{K_2} d\Sigma, \quad D_{2k}^{Nw} \\ &= \int_\Sigma k_2 Q_{44} X_1^{K_1} X_2^{K_2 - 1} d\Sigma, \quad D_{3k}^{Nw} = \int_\Sigma k_1 Q_{35} X_1^{K_1 - 1} X_2^{K_2} d\Sigma \end{aligned} \tag{A.5}$$

(no sum on k_1, k_2)

$$\mathbf{D}^{Nw'} = \left[D_{ik}^{Nw'} \right] \quad i = 1,2,3; \quad k = 1,2,\ldots,m_w$$

$$\begin{aligned} D_{1k}^{Nw'} &= \int_\Sigma Q_{53} \frac{X_1^{K_1} X_2^{K_2}}{J} d\Sigma, \quad D_{2k}^{Nw'} = 0, \quad D_{3k}^{Nw'} \\ &= \int_\Sigma Q_{33} \frac{X_1^{K_1} X_2^{K_2}}{J} d\Sigma \end{aligned} \tag{A.6}$$

$$\mathbf{D}^{M\Theta} = \begin{bmatrix} \int_\Sigma Q_{53} \frac{X_2^2}{J} d\Sigma & -\int_\Sigma Q_{33} \frac{X_1 X_2}{J} d\Sigma & -\int_\Sigma Q_{35} \frac{X_2^2}{J} d\Sigma \\ & \int_\Sigma Q_{33} \frac{X_1^2}{J^2} d\Sigma & \int_\Sigma Q_{44} \frac{X_1 X_2}{J} d\Sigma \\ Sym & & \int_\Sigma \left(Q_{44} \frac{X_1^2}{J} + Q_{55} \frac{X_2^2}{J} \right) d\Sigma \end{bmatrix} \tag{A.7}$$

$$\mathbf{D}^{M\Gamma} = \begin{bmatrix} \int_\Sigma Q_{33} \frac{X_1^2 X_2}{J^2} d\Sigma & \int_\Sigma Q_{33} \frac{X_2^3}{J} d\Sigma & -\int_\Sigma Q_{33} \frac{X_1 X_2^2}{J^2} d\Sigma \\ -\int_\Sigma Q_{33} \frac{X_1^3}{J^2} d\Sigma & -\int_\Sigma Q_{33} \frac{X_1 X_2^2}{J^2} d\Sigma & \int_\Sigma Q_{33} \frac{X_1^2 X_2}{J^2} d\Sigma \\ -\int_\Sigma Q_{53} \frac{X_1^2 X_2}{J^2} d\Sigma & -\int_\Sigma Q_{53} \frac{X_2^3}{J^2} d\Sigma & \int_\Sigma Q_{53} \frac{X_1 X_2^2}{J^2} d\Sigma \end{bmatrix} \tag{A.8}$$

$$\begin{aligned} &\mathbf{D}^{Mw} = \left[D_{ik}^{Mw} \right] i = 1,2,3; \quad k = 1,2,\ldots,m_w \\ &D_{1k}^{Mw} = \int_\Sigma k_1 Q_{35} X_1^{K_1 - 1} X_2^{K_2 + 1} d\Sigma \text{ (no sum on } k_1) \\ &D_{2k}^{Mw} = -\int_\Sigma k_1 Q_{35} X_1^{K_1} X_2^{K_2} d\Sigma \\ &D_{3k}^{Mw} = \int_\Sigma k_1 Q_{44} X_1^{K_1 - 1} X_2^{K_2 - 1} d\Sigma - \int_\Sigma k_1 Q_{55} X_1^{K_1 - 1} X_2^{K_2 + 1} d\Sigma \text{ (no sum on } k_1, \ k_2) \\ &\mathbf{D}^{Mw'} = \left[D_{ik}^{Mw'} \right] i = 1,2,3; \quad k = 1,2,\ldots,m_w \end{aligned} \tag{A.9}$$

$$D_{1k}^{Mw'} = \int_\Sigma Q_{44}\frac{X_1^{K_1}X_2^{K_2+1}}{J}d\Sigma, \quad D_{2k}^{Mw'} = -\int_\Sigma Q_{33}\frac{X_1^{K_2+1}X_2^{K_2}}{J}d\Sigma, \quad D_{3k}^{Mw'} = -\int_\Sigma Q_{53}\frac{X_1^{K_1}X_2^{K_2+1}}{J}d\Sigma \tag{A.10}$$

$$\mathbf{D}^{P\Gamma} = \begin{bmatrix} \int_\Sigma Q_{33}\frac{X_1^4}{J^3}d\Sigma & \int_\Sigma Q_{33}\frac{X_1^2X_2^2}{J^3}d\Sigma & -\int_\Sigma Q_{33}\frac{X_1^3X_2}{J^3}d\Sigma \\ & \int_\Sigma Q_{33}\frac{X_2^4}{J^3}d\Sigma & -\int_\Sigma Q_{33}\frac{X_1X_2^3}{J^3}d\Sigma \\ Sym & & \int_\Sigma Q_{33}\frac{X_1^2X_2^2}{J^3}d\Sigma \end{bmatrix} \tag{A.11}$$

$$\mathbf{D}^{Pw} = \left[D_{ik}^{Pw}\right] i = 1,2,3; \quad k = 1,2,\ldots,m_w$$

$$D_{1k}^{Pw} = \int_\Sigma k_1 Q_{35}\frac{X_1^{K_1+1}X_2^{K_2}}{J}d\Sigma, \quad D_{2k}^{Pw} = \int_\Sigma k_1 Q_{35}\frac{X_1^{K_2-1}X_2^{K_2+2}}{J}d\Sigma, \quad D_{3k}^{Pw} = -\int_\Sigma k_1 Q_{35}\frac{X_1^{K_1}X_2^{K_2+1}}{J}d\Sigma \tag{A.12}$$

(no sum on k_1)

$$\mathbf{D}^{Pw'} = \left[D_{ik}^{Pw'}\right] i = 1,2,3; \quad k = 1,2,\ldots,m_w$$

$$D_{1k}^{Pw'} = \int_\Sigma Q_{33}\frac{X_1^{K_1+2}X_2^{K_2}}{J_2}d\Sigma, \quad D_{2k}^{Pw'} = \int_\Sigma Q_{33}\frac{X_1^{K_1}X_2^{K_2+2}}{J}d\Sigma, \quad D_{3k}^{Pw'} = -\int_\Sigma Q_{33}\frac{X_1^{K_1+1}X_2^{K_2+1}}{J}d\Sigma \tag{A.13}$$

$$\mathbf{D}^{vw} = \left[D_{ik}^{vw}\right] i = 1,2,3; \quad k = 1,2,\ldots,m_w$$

$$D_{hk}^{vw} = \int_\Sigma h_1 k_1 Q_{55} X_1^{h_1+K_1-2}X_2^{h_2+K_2}Jd\Sigma + \int_\Sigma h_2 k_1 Q_{44} X_1^{h_1+K_1}X_2^{h_2+K_2-2}Jd\Sigma \text{ (no sum on } h_1,\ h_2,\ k_1, k_2) \tag{A.14}$$

$$\mathbf{D}^{vw'} = \left[D_{hk}^{vw'}\right] h,k = 1,2,\ldots,m_w$$

$$D_{hk}^{vw'} = \int_\Sigma h_1 Q_{53} X_1^{h_1+K_1-1}X_2^{h_2+K_2}d\Sigma \text{ (no sum on } h_1) \tag{A.15}$$

Appendix B

Let us compute the derivative of the stiffness matrix defined by Eq. (27). Accounting for the symmetry of the bilinear form $\mathbf{B}_L(\mathbf{U}_e)\cdot\Delta\mathbf{U}_e$, we easily obtain the equation

$$D(\mathbf{B}_L(\mathbf{U}_e)\mathbf{U}_e)\Delta\mathbf{U}_e = 2\mathbf{B}_L(\mathbf{U}_e)\Delta\mathbf{U}_e \tag{B.1}$$

which can also be written as

$$\left[D\mathbf{B}_L^T(\mathbf{U}_e)\Delta\mathbf{U}_e\right]\widehat{\mathbf{S}}(\mathbf{U}_e) = \mathbf{G}^T\widetilde{\mathbf{S}}(U_e)\mathbf{G}\Delta\mathbf{U}_e \tag{B.2}$$

where $\widetilde{S}$ is the following 9×9 symmetric matrix

$$\begin{bmatrix} sN_3 & 0 & 0 & 0 & \frac{M_1}{R} & -N_2 & 0 & 0 & -M_1 \\ & N_3 & \frac{N_3}{R} & 0 & \frac{M_2}{R} & N_1 & 0 & 0 & -M_2 \\ & & \frac{N_3}{R} & 0 & \frac{M_2}{R^2} & \frac{N_1}{R} & 0 & 0 & -\frac{M_2}{R} \\ & & & 0 & \frac{M_2}{2R} & \left(\frac{N_1}{2}-\frac{M_3}{2R}\right) & 0 & -\frac{M_3}{2} & -\frac{M_2}{2} \\ & & & & \left(-\frac{M_1}{R}+\frac{P_1+P_2}{R^2}\right) & \frac{N_2}{2} & \frac{M_3}{2} & 0 & \left(\frac{M_1}{2}-\frac{P_1+P_2}{R}\right) \\ & & & & & \left(\frac{M_1}{R}+\frac{P_1}{R^2}\right) & \left(-\frac{M_2}{2}+\frac{P_3}{R}\right) & \left(\frac{M_1}{2}+\frac{P_1}{R}\right) & 0 \\ & & & & & & P_2 & P_3 & 0 \\ & & Sym & & & & & P_1 & 0 \\ & & & & & & & & (P_1+P_2) \end{bmatrix} \tag{B.3}$$

By discarding second-order terms, we hence obtain:

$$D\mathbf{K}_e(\mathbf{U})_e\Delta\mathbf{U}_e = [\mathbf{K}_{0_e} + \mathbf{K}_{L_e}(\mathbf{U}_e) + \mathbf{K}_{G_e}(\mathbf{U}_e)]\Delta\mathbf{U}_e \tag{B.4}$$

where

$$\mathbf{K}_{0_e} = \int_{-1}^{1}\mathbf{B}_0^T\widehat{\mathbf{D}}\mathbf{B}_0 G d\xi \tag{B.5}$$

$$\mathbf{K}_{L_e}(\mathbf{U}_e) = \int_{-1}^{1}\left[\mathbf{B}_0^T\widehat{\mathbf{D}}\mathbf{B}_L(\mathbf{U}_e) + \mathbf{B}_L^T(\mathbf{U}_e)\widehat{\mathbf{D}}\mathbf{B}_0 + \mathbf{B}_L^T(\mathbf{U}_e)\widehat{\mathbf{D}}\mathbf{B}_L(\mathbf{U}_e)\right]Gd\xi \tag{B.6}$$

$$\mathbf{K}_{G_e}(\mathbf{U}_e) = \int_{-1}^{1}\mathbf{G}^T\widetilde{\mathbf{S}}(\mathbf{U}_e)\mathbf{G} \quad Gd\xi \tag{B.7}$$

are the initial stiffness matrix; initial displacement stiffness matrix; and geometric stiffness matrix of the current element, respectively.

We compute now the derivative of the element second-order force vector $\mathbf{Q}_e^{(2)}(\mathbf{U}_e)$ defined in Eq. (26)$_2$, obtaining

$$\mathbf{K}_{Q_e} = D\mathbf{Q}_e^{(2)}(\mathbf{U}_e)\Delta\mathbf{U}_e = \int_{-1}^{1}\mathbf{N}^T\widehat{\mathbf{C}}\mathbf{N}\Delta\mathbf{U}_e G d\xi \tag{B.8}$$

where

$$\widehat{\mathbf{C}}_{[m\times m]} = \begin{bmatrix} \mathbf{0} & \mathbf{0} & \mathbf{0} \\ \mathbf{0} & \widehat{\widehat{\mathbf{C}}} & \mathbf{0} \\ \mathbf{0} & \mathbf{0} & \mathbf{0} \end{bmatrix} \tag{B.9}$$

$$\widehat{\widehat{\mathbf{C}}}_{[3\times 3]} = \begin{bmatrix} -C_{22} & \frac{1}{2}(C_{12}+C_{21}) & \frac{1}{2}C_{31} \\ \frac{1}{2}(C_{12}+C_{21}) & C_{11} & \frac{1}{2}C_{32} \\ \frac{1}{2}C_{31} & \frac{1}{2}C_{32} & -(C_{11}+C_{22}) \end{bmatrix} \tag{B.10}$$

with C_{ij} being the components of the second-order tensor $\mathbf{C}$ defined in [35].

For what concerns the second-order nodal force vectors, we obtain

$$D\mathbf{Q}_I^{(2)}(\hat{\mathbf{u}}_I)\Delta\hat{\mathbf{u}}_I = \widehat{\mathbf{C}}_I\Delta\hat{\mathbf{u}}_I \tag{B.11}$$

where

$$\underset{[m\times m]}{\widehat{\mathbf{C}}_1} = \begin{bmatrix} \mathbf{0} & \mathbf{0} & \mathbf{0} \\ \mathbf{0} & \widehat{\widehat{\mathbf{C}}}_\mathbf{I} & \mathbf{0} \\ \mathbf{0} & \mathbf{0} & \mathbf{0} \end{bmatrix} \tag{B.12}$$

$$\underset{[3\times 3]}{\widehat{\widehat{\mathbf{C}}}_I} = \begin{bmatrix} -C_{I_{22}} & \frac{1}{2}(C_{I_{12}}+C_{I_{21}}) & \frac{1}{2}C_{I_{31}} \\ \frac{1}{2}(C_{I_{12}}+C_{I_{21}}) & C_{I_{11}} & \frac{1}{2}C_{I_{32}} \\ \frac{1}{2}C_{I_{31}} & \frac{1}{2}C_{I_{32}} & -(C_{I_{11}}+C_{I_{22}}) \end{bmatrix} \tag{B.13}$$

with $C_{I_{ij}}$ being the components of the second-order tensors C_I defined in [35].

The total tangent stiffness matrix of the generic element is therefore given by

$$\mathbf{K}_T(\mathbf{U},\lambda) = \mathbf{K}_o + \mathbf{K}_L(\mathbf{U}) + \mathbf{K}_G(\mathbf{U}) - \lambda\mathbf{K}_Q \tag{B.14}$$

where $\mathbf{K}_0$, $\mathbf{K}_L$ and $\mathbf{K}_G$ are the global versions of the matrices defined by Eqs. (B.5)–(B.7); while $\mathbf{K}_Q$ is the load-correction matrix deriving

by the assembly of the element matrices (B.8), and the nodal matrices (B.11). From equation (B.14), we easily deduce:

$$D_\lambda \mathbf{K}_T(\mathbf{U},\lambda)\mathbf{V} = -\mathbf{K}_Q\mathbf{V} \tag{B.15}$$

We end by computing the generic element contributions to the $\mathbf{h}_i$ vectors introduced in Eq. (44) of the main paper (i = 1,2.3). Making use of Eqs. (B.4)–(B.8), (B.15), and discarding second-order terms, we obtain

$$\mathbf{h}_{e_j} = -\int_{-1}^{+1}\left\{\left[\mathbf{B}_0^T + \mathbf{B}_L(\mathbf{U}_e)\right]^T \widehat{\mathbf{D}}\mathbf{B}_L(\Delta\mathbf{U}_{e_j}) + \mathbf{B}_L^T(\Delta\mathbf{U}_{e_j})\widehat{\mathbf{D}}\left[\mathbf{B}_0 + \mathbf{B}_L^T(\mathbf{U}_{e_j})\right] + \mathbf{G}^T\Delta\widetilde{\mathbf{S}}_j\mathbf{G}\right\}\mathbf{V}_E G d\xi \quad (j=1,2,3) \tag{B.16}$$

where $\Delta\widetilde{\mathbf{S}}_j$ is a 9×9 matrix obtained through Eq. (B.3), by replacing the generalized stresses $\widehat{\mathbf{S}}$ with the incremental stresses

$$\Delta\widehat{\mathbf{S}}_j = \widehat{\mathbf{D}}[\mathbf{B}_0 + \mathbf{B}_L(\mathbf{U}_{e_j})]\Delta\mathbf{U}_{e_j} \tag{B.17}$$

References

[1] Ascione L, Feo L, Fraternali F. Load carrying capacity of 2D FRP/strengthened masonry structures. Compos Part B: Eng 2005;36:619–26.
[2] Ascione L, Berardi VP. Anchorage device for FRP laminates in the strengthening of concrete structures close to beam-column joints. Compos Part B: Eng 2011;42(7):1840–50.
[3] Ascione L, Mancusi G, Spadea S. Flexural behaviour of concrete beams reinforced with GFRP bars. Strain 2010;46:460–9.
[4] Adanur S, Mosallam AS, Shinozuka M, Gumusel L. A comparative study on static and dynamic responses of FRP composite and steel suspension bridges. J Reinf Plast Compos 2011;30(15):1265–79.
[5] Bai Y, Keller T. Modal parameter identification for a GFRP pedestrian bridge. Compos Struct 2008;82(1):90–100.
[6] Mendes PJD, Barros JAO, Sena-Cruz JM, Taheri M. Development of a pedestrian bridge with GFRP profiles and fiber reinforced self-compacting concrete deck. Compos Struct 2011;93(11):2969–82.
[7] Fraternali F, Ciancia V, Chechile R, Rizzano G, Feo L, Incarnato L. Experimental study of the thermo-mechanical properties of recycled PET fiber reinforced concrete. Compos Struct 2011;93:2368–74.
[8] Fraternali F, Farina I, Polzone C, Pagliuca E, Feo L. On the use of R-PET strips for the reinforcement of cement mortars. Compos Part B: Eng 2012;46:207–10.
[9] Bencardino F, Rizzuti L, Spadea G, Swamy RN. Implications of test methodology on post-cracking and fracture behaviour of Steel Fibre Reinforced Concrete. Compos Part B: Eng 2013;46:31–8.
[10] Ascione L, Fraternali F. A penalty model for the analysis of composite curved beams. Comput Struct 1992;45:985–99.
[11] Fraternali F, Reddy JN. A penalty model for the analysis of laminated composite shells. Int J Solids Struct 1993;30:3337–55.
[12] Razaqpur AG, Li H. Refined analysis of curved thin-walled multicell box-girder. Comput Struct 1994;53(1):131–42.
[13] Segura JM, Armengaud G. Analytical formulation of stresses in curved composite beams. Arch Appl Mech 1998;68(3–4):206–13.
[14] Kapania RK, Li J. A formulation and implementation of geometrically exact curved beam elements incorporating finite strains and finite rotations. Comput Mech 2003;30(5–6):444–59.
[15] Chang C, Hodges DH. Stability studies for curved beams. J Mech Mater Struct 2009;4(7–8):1257–70.
[16] Ecsedi I, Dluhi K. A linear model for the static and dynamic analysis of non-homogeneous curved beams. Appl Math Modell 2005;29(12):1211–31.
[17] Dagher HJ, Bannon DJ, Davids WG, Lopez-Anido RA, Nagy E, Goslin K. Bending behavior of concrete-filled tubular FRP arches for bridge structures. Construct Build Mater 2012;37:432–9.
[18] Jung W, Park J, Kim S. A study on the behavior characteristics of curved FRP-concrete composite panel. Adv Mater Res 2012:375–80.
[19] Roberts TM. Influence of shear deformation on buckling of pultruded fiber reinforced plastic profiles. J Compos Construct 2002;6(4):241–8.
[20] Ascione L, Giordano A, Spadea S. Lateral buckling of pultruded FRP beams. Compos Part B: Eng 2011;42(4):819–24.
[21] Ascione L, Berardi VP, Giordano A, Spadea S. Local buckling behavior of FRP thin-walled beams: a mechanical model. Compos Structu 2013;98:111–20.
[22] Ascione L, Berardi VP, Giordano A, Spadea S. Buckling failure modes of FRP thin-walled beams. Compos Part B: Eng 2013;47:357–64.
[23] Feo L, Fraternali F. On a moderate rotation theory of thin-walled composite beams. Compos Part B: Eng 2000;31:141–58.
[24] Roberts TM, Al-Ubaidi H. Influence of shear deformation on restrained torsional warping of pultruded FRP bars of open cross-section. Thin-Wall Struct 2001;39:395–414.
[25] Feo L, Mancusi G. Modeling shear deformability of thin-walled composite beams with open cross-section. Mech Res Commun 2010;37(3):320–5.
[26] Viera RF, Virtuoso FBE, Pereira, EBR. A Higher order thin-walled beam model including warping and shear modes. Int J Mech Sci. http://dx.doi.org/10.1016/j.ijmecsci.2012.10.009.
[27] Carrera E, Petrolo M. On the effectiveness of higher-order terms in refined beam theories. J Appl Mech 2011:78.
[28] Sun J, Zhu H, Qin S, Yang D, He X. A review on the research of mechanical problems with different moduli in tension and compression. J Mech Sci Technol 2010;24(9):1845–54.
[29] Bert CW. Models for fibrous composites with different properties in tension and compression. J Eng Mater Technol. ASME Ser H 1977;99(4):344–9.
[30] Conners TE, Medvecz PJ. Wood as a bimodular material. Institute of Paper Science and Technology – Technical Paper No. 423, Atlanta, Georgia; 1992.
[31] Markkula S, Malecki HC, Zupan M. Uniaxial tension and compression characterization of hybrid CNS-glass fiber-epoxy composites. Compos Struct 2013;95:337–45.
[32] Fraternali F. Free discontinuity finite element models in two-dimensions for in-plane crack problems. Theor Appl Fract Mech, 0167-8442 2007;47:274–82. http://dx.doi.org/10.1016/j.tafmec.2007.01.006.
[33] Schmidt B, Fraternali F, Ortiz M. Eigenfracture: an eigendeformation approach to variational fracture. Siam J Multisc Model Simul 2009;7(3):1237–66.
[34] Fraternali F, Negri M, Ortiz M. On the convergence of 3D free discontinuity models in variational fracture. Int J Fract 2010;166(1–2):3–11.
[35] Fraternali F, Bilotti G. Nonlinear elastic stress analysis in curved composite beams. Comput Struct 1997;62(5):837–59.
[36] Batoz JL, Dhatt G. Incremental displacement algorithms for non-linear problems. Int J Numer Methods Eng 1979;14:1262–7.
[37] Keller HB. Numerical solution of bifurcation and nonlinear eigenvalue problems. In: Rabinowitz P, editor. Applications of bifurcation theory. New York: Academic Press; 1977. p. 359–84.
[38] Simo JC, Wriggers P. A general procedure for the direct computation of turning and bifurcation points. Int J Numer Methods Eng 1990;30:155–76.
[39] Timoshenko SP, Gere JM. Theory of elastic stability. New York: McGraw-Hill; 1961.
[40] Dawe. A finite deflection analysis of shallow arches. Int J Numer Methods Eng 1971;3(4):529–52.
[41] Bruno D, Lato S, Sacco E. Nonlinear analysis of bimodular composite plates under compression. Comput Mech 1994;14(1):28–37.
[42] Nomizu K, Kobayashi S. Foundations of differential geometry. New York: Wiley; 1963.
[43] Budiansky B. Theory of buckling and post-buckling behaviour of elastic structure. In: Yih Chia-Shun, editor. Advances in applied mechanics, vol. 14. New York: Academic Press; 1974. p. 1–65.
[44] Cyron CJ, Arrojo M, Ortiz M. Smooth, second-order, non-negative meshfree approximants selected by maximum entropy. Int J Numer Methods Eng 2009;79:1605–32.
[45] Fraternali F, Lorenz C, Marcelli G. On the estimation of the curvatures and bending rigidity of membrane networks via a local maximum-entropy approach. J Comput Phys 2012;231:528–40.
[46] Schmidt B, Fraternali F. Universal formulae for the limiting elastic energy of membrane networks. J Mech Phys Solids 2012;60:172–80.
[47] Fraternali F, Angelillo M, Fortunato A. A lumped stress method for plane elastic problems and the discrete-continuum approximation. Int J Solids Struct 2002;39:6211–40.